Supporting Information

Anderson et al. 10.1073/pnas.1503348112

SI Materials and Methods

Brain Slices. Male or female mice (postpartum days 18–26) were deeply anesthetized with isoflurane and decapitated. Brains were quickly removed and sectioned into 210-μm-thick coronal slices containing the DCN using a vibratome (VT-1200S; Leica). Slices were incubated in carbogenated artificial cerebrospinal fluid (ACSF) containing (in millimolar) NaCl 127, KCl 3, $CaCl_2$ 2.4, $MgCl_2$ 1.3, $NaHCO_3$ 21, Hepes 3.5, and glucose 25, pH ∼7.4, ∼310 mOsm) at 35 °C for 1 h before being placed into the recording chamber. Experiments using ZnT3 KO mice were performed blind to the genotype of the animal. In preparing the ACSF used to measure NMDAR currents and tonic zinc, we removed contaminating zinc from our solutions with Chelex 100 resin (Biorad). After applying Chelex to the ACSF, high-purity calcium and magnesium salts were added (99.995% purity; Sigma-Aldrich). All plastic and glassware was washed with 5% high-purity nitric acid (Sigma-Aldrich).

Electrophysiological Recordings. Whole-cell recordings from cartwheel cells in DCN slices were obtained with glass micropipettes (4–7 MΩ) filled with a cesium-based internal solution containing (in millimolar) $Cs(CH_3O_3S)$ 126, KCl 4, Hepes 10, Na_2ATP 4, Tris-GTP 0.3, Tris-phosphocreatine 10, CsEGTA 1, QX-314 1, sodium ascorbate 3, Alexa-594, 0.01, pH = 7.25, 295 mOsm. Cartwheel cells were identified by the presence of complex spikes in cell-attached configuration before break-in and by the morphology of their dendritic arbors visualized with Alexa-594 after completion of the recording. Using ephus (1) and a Multiclamp 700B amplifier (Axon Instruments), NMDAR EPSCs were recorded in voltage clamp mode in the presence of DNQX (20 μM, AMPAR and kainate receptor antagonist), SR95531 (20 μM, $GABA_AR$ antagonist), and strychnine (1 μM, GlyR antagonist). NMDAR EPSCs were evoked by parallel fiber stimulation with voltage pulses through a theta glass electrode. To confirm that the EPSCs were mediated by NMDARs, at the end of each experiment, AP5 (50 μM, a specific NMDAR antagonist) was applied. Recordings were performed at room temperature unless stated otherwise. The series resistance was not compensated and was monitored during the recording by delivering −5 mV voltage steps for 50 msec. Recordings were excluded from further analysis if the series resistance changed by more than 20% compared to the baseline period. Data were low-pass-filtered at 4 kHz and sampled at 10 kHz. NMDAR EPSC peak values were averaged over a 20-ms time window. Because zinc affects the decay kinetics of NMDARs (2, 3), we measured the decay kinetics of NMDAR EPSCs (Table S1) in the presence of the high-affinity, fast zinc chelator ZX1 (4) (100 μM). The decay time of NMDAR EPSCs were fit with

$$I(t) = I_f * e^{(-t/\tau_f)} + I_s * e^{(-t/\tau_s)} + c, \quad \text{[S1]}$$

where I_f and I_s are the amplitudes of the fast and slow components of the response, τ_f and τ_s are the time constants of the fast and slow components of the NMDAR EPSC, and c is the offset. The weighted time constant (τ_w) of each NMDAR EPSC was calculated with

$$\tau_w = \tau_f * \frac{I_f}{(I_f + I_s)} + \tau_s * \frac{I_s}{(I_f + I_s)}, \quad \text{[S2]}$$

where τ_f and τ_s are the fast and slow time constants from Eq. **S1** and I_f and I_s are the amplitudes of the fast and slow components of the current from Eq. **S1**. To measure ifenprodil sensitivity of these NMDARs, we calculated the IC_{50} of ifenprodil with the Hill equation,

$$Y = \frac{B_{max}}{1 + 10^{(log(IC_{50}) - x)*h}}, \quad \text{[S3]}$$

where B_{max} is the maximum inhibition of ifenprodil, h is the Hill coefficient, and IC_{50} is the dose of ifenprodil that achieved 50% of the maximum inhibition of the NMDAR EPSC.

Glutamate Uncaging. Cartwheel cells were targeted for whole-cell recordings as stated above, but with tetrodotoxin (TTX, 500 nM) in the ACSF to prevent action potentials. To activate NMDARs, we photolytically uncaged 4-Methoxy-7-nitroindolinyl (MNI)-caged glutamate (100 μM) onto the dendritic arbor in the molecular layer using 1- or 2-ms pulses of UV-laser light (355 nm; DPSS Lasers). Laser power, duration, and uncaging location were adjusted so that the evoked NMDAR current reached a peak amplitude of about 150 pA. Once a stable uncaging response was established, we added ZX1 to the ACSF to measure the effect of tonic zinc chelation on the uncaging-evoked NMDAR current.

Fluorescence Imaging. We synthesized 6-CO_2H ZP1 (5) linked to lissamine rhodamine B (LRB) (LZ9, see below) for ratiometric imaging of extracellular zinc levels. To measure tonic zinc levels, slices were incubated in recirculating ASCF containing the fluorescent ratiometric zinc sensor LZ9 (2 μM) and blockers of ionotropic receptors (AP5, 50 μM; SR95331, 20 μM; DNQX, 20 μM, and strychnine, 1 μM) to reduce activity-dependent autofluorescence (6). Because of the large FRET component of this ratiometric zinc sensor [red emission from LRB via Foerster resonance energy transfer (FRET) excitation by ZP1, Fig. S7 *A* and *B*], we used an interleaved, multiplexed approach for ratiometric imaging. Blue excitation of LZ9 excites the ZP1 moiety, so all emission wavelengths, green or red, are due to the zinc-sensitive component of the sensor. Green excitation of LZ9 excites LRB, resulting in zinc-insensitive red emission. Using ephus, blue and green light-emitting diodes (M470L2 and M530L2; Thorlabs) were synchronized with the exposure times of a CCD camera (Rolera XR; QImaging) so that every other frame used either blue or green excitation. A Pinkel filter set was used to separate the two emission and two excitation colors (LF488/543/635-3X-A-000; Semrock). Two-channel, multiplexed movies were acquired using an upright microscope (Olympus BX5) with a 20× or 40× water immersion objective and epifluorescence optics. To measure tonic zinc levels in DCN slices, "time-lapse" movies were acquired so that each pair of frames (paired blue and green excitation) was separated by 30 s. This imaging approach allowed us to monitor the fluorescence responses for 30 min or more. Thus, we ensured that fluorescence values had reached a steady state for accurate measurements of the tonic fluorescence before calibrating the probes with EDTA and $ZnCl_2$. The ratio of ZP1-based fluorescence to LRB-based fluorescence (ratiometric zinc signal, R) was created by dividing the frame-averaged region of interest (ROI) during blue excitation by the same ROI in the subsequent frame acquired with green excitation for each pair of frames. For each experiment, LZ9 was calibrated by adding 4.5 mM of the high-affinity zinc chelator EDTA to the ACSF to measure R_{min} followed by 5 mM $ZnCl_2$ to saturate the probe and measure R_{max}. Based on R_{min}

and R_{max}, each ratiometric frame was converted into zinc concentration using

$$[Zn^{2+}] = K_d * \frac{(R - R_{min})}{(R_{max} - R)}, \quad \text{[S4]}$$

where K_d is the dissociation constant of the ratiometric probe and R is the ratiometric fluorescence acquired with interleaved multiplexed imaging (7). R_{min} is the minimum ratiometric fluorescence of the probe in the presence of EDTA and R_{max} is the maximum fluorescence with saturating levels of $ZnCl_2$. The dynamic range (8) of each probe was calculated with

$$\text{Dynamic Range} = \frac{F_{max} - F_{min}}{F_{min}} \times 100. \quad \text{[S5]}$$

The percent probe saturation by tonic zinc levels was calculated with

$$\text{Percent Probe Saturation by Tonic Zinc} = \frac{(F_{tonic} - F_{min})}{(F_{max} - F_{min})} \times 100, \quad \text{[S6]}$$

where F_{tonic} is the baseline fluorescence level caused by tonic zinc. F_{min} is the minimum fluorescence measured in the presence of EDTA and F_{max} is the maximum fluorescence with saturating levels of $ZnCl_2$.

For synaptic zinc release imaging experiments, 200 μM CaEDTA was added to the ACSF 20 min before imaging instead of using Chelex pretreatment and the temperature of the ACSF was raised to 31–33 °C with an inline heater (Warner). Two-channel, multiplexed movies were acquired as above, but at frame rates of 20 Hz, each channel at a frame rate of 10 Hz. Each frame had an exposure time of 38 ms, and the interframe interval was 50 ms. Synaptic zinc release was evoked with a theta-stimulating electrode using multiple stimulus intensities: 2, 10, 20, 30, 50, 100, 150, and 200 pulses delivered at 100 Hz. To visualize the location of the fluorescent response, a fourth order, low-pass, two-dimensional Butterworth filter was applied to each frame. This revealed a "hotspot" of fluorescence in the molecular layer of the DCN and this ROI was quantified in the unfiltered images.

Data Analysis. All analysis was performed with custom routines in MATLAB (The MathWorks), with Dynafit (Biokin), or with Prism5 (GraphPad). For statistical comparisons, if the group data passed the Lilliefor's test for normality, Student's *t* tests were used to assess significance; otherwise Wilcoxon rank sum tests were used. Paired data were compared using paired *t* tests, or ANOVA. Electrophysiological group data are presented as mean ± SEM; significance levels are defined as $P < 0.05$. Cuvette-based fluorescence group data are presented as mean ± SD. Kinetic traces of fluorescence turn-off were fit with

$$F(t) = (F_o - F_{min}) * e^{(-t * k_{obs})} + F_{min}, \quad \text{[S7]}$$

where $F(t)$ is the initial fluorescence value, F_{min} is the minimal fluorescence value, t is time, and k_{obs} is the observed first-order rate constant in units of 1/time (s^{-1}). Kinetic traces of ligand binding were fit with

$$F(t) = F_o * \frac{F_{max} - F_o}{1 - e^{-k/t}}, \quad \text{[S8]}$$

where the F_{max} is the maximum fluorescence intensity, F_o is the initial fluorescence intensity, t is time, and k is the rate constant in units of 1/time (s^{-1}).

Reagents for Electrophysiological Experiments. Salts for ACSF and internal solution were purchased from Sigma-Aldrich. ZX1 was either synthesized (4) or purchased from Strem Chemicals. Newport Green was purchased from Invitrogen. CaEDTA was prepared fresh for each experiment by combing 1 M $CaCl_2$ with 1 M EDTA and allowing the solution to equilibrate for at least 30 min. SR95531, strychnine, DNQX, AP5, QX-314, TTX, and CPP were purchased from Abcam. MNI-glutamate and TBOA were purchased from Tocris Bioscience. D-AA was purchased from Sigma.

Reagents. HPLC-grade acetonitrile, anhydrous *N*,*N*-dimethylformamide (DMF), dichloromethane, 4-methylpiperidine, *N*,*N*-diisopropylethylamine (DIPEA), ≥99% (titration) *N*-[Tris(hydroxymethyl) methyl]glycine (tricine), potassium hydroxide, and all metal salts were purchased from Sigma-Aldrich. 2-(7-Aza-1*H*-benzotriazole-1-yl)-1,1,3,3-tetramethyluronium hexafluorophosphate (HATU) was procured from Oakwood Chemicals. Fmoc-Glu(OtBu)-Wang resin and Fmoc-Lys(MTT)-OH were obtained from Aapptec. Fmoc-Pro-OH was obtained from Novabiochem. Hoechst 33258 stain was purchased from Life Technologies. All solvents and commercial reagents were used as received. 6-CO_2H Zinpyr-1 and LRB sulfonyl chloride were prepared according to literature procedures (5, 9); 2,4-DPA [(2-picolyl)(4-picolyl)amine] was synthesized as previously described (10). An Agilent Technologies 1200 series HPLC system equipped with a multiwavelength detector, automated injector, and thermostated fraction collector was used to purify LZ9 and 7-hydroxy-2-oxo-8-(((pyridin-2-ylmethyl) (pyridin-4-ylmethyl)amino)methyl)-2*H*-chromene-3-carboxylic acid (3-CO_2H CM2). The purity of LZ9 and 3-CO_2H CM2 was assessed by analytical HPLC on a similar instrument. Mass spectra [electrospray ionization (ESI)-MS] were collected on an 1100 series Agilent LC/MSD ion trap with a mobile phase composed of methanol, water, and formic acid (49.95, 49.95, 0.1%, vol/vol). High-resolution mass spectrometry (HR-ESI-MS) was conducted by staff at the Massachusetts Institute of Technology Department of Chemistry Instrumentation Facility on a Bruker Daltonics APEXIV 4.7 T Fourier transform ion cyclotron resonance MS instrument. NMR spectra were acquired on a Varian Inova 500 spectrometer; ^{1}H NMR chemical shifts are reported in parts per million relative to $SiMe_4$ (δ = 0) and were referenced internally with respect to residual protons in the solvent (δ 2.50 for DMSO-d_6). Coupling constants are reported in hertz. Aqueous solutions were prepared using deionized water from a Millipore purification system (resistivity = 18.2 MΩ cm). Molecular biology grade PIPES and 99.999% KCl were purchased from Aldrich. All buffered solutions were treated with Chelex resin (Bio-Rad) according to manufacturer specifications. Stock solutions of tricine were prepared by dissolving a known amount in Milli-Q water and adjusting the pH to 7.0 using potassium hydroxide. A 100 mM $ZnSO_4$ solution (Sigma-Aldrich) was used for UV-visible and fluorescence spectroscopy and kinetic studies. A 100 mM $ZnCl_2$ solution (Sigma-Aldrich) was used for potentiometric titrations. A 50 mM zinc(II) stock solution was prepared using 99.999% anhydrous $ZnCl_2$ (Aldrich). Stock solutions for metal ion selectivity tests were prepared using 99.9% anhydrous $MgCl_2$ (Aldrich), 99.99% anhydrous $MnCl_2$ (Alfa Aesar), 99.5% anhydrous $CoCl_2$ (Sigma-Aldrich), 98% $NiCl_2{\cdot}6\,H_2O$ (Aldrich), 98% $CuCl_2{\cdot}6\,H_2O$ (Alfa Aesar), 99.9% anhydrous $CaCl_2$ (Aldrich), and 99.999% anhydrous $CdCl_2$ (Aldrich). UV-visible spectra were recorded on a Varian Cary 50 Bio UV-visible spectrophotometer. Fluorescence spectra were recorded on a Quanta Master 4 L-format scanning spectrofluorimeter (Photon Technology International). The acquisition temperature was kept constant by a circulating water bath. Sample solutions were placed in quartz cuvettes (Starna) with 1-cm path lengths.

LZ9 Synthesis. The peptide scaffold, P_9KE, was synthesized by an Aapptec Focus Xi automated peptide synthesizer on the 75-μmol scale using Fmoc-Glu(OtBu) Wang resin. Fmoc groups were removed by treating the resin with a solution of 20% (vol/vol) 4-methylpiperidine in DMF. For typical coupling reactions, a 4.5-mL coupling solution was freshly prepared consisting of equal parts 0.2 M Fmoc-protected amino acid in DMF, 0.2 M HATU in DMF, and 1 M DIPEA in 10% (vol/vol) CH_2Cl_2 in DMF. The resin was allowed to react in the coupling solution for 30 min. After synthesis of the peptide scaffold was complete, the resin was transferred to a 5-mL disposable polypropylene syringe (Torviq) equipped with a porous polypropylene disk. Fluorophores were added manually using a modified literature procedure (11). First, LRB was appended to the N terminus by reacting the resin with 1.5 mL of a 0.1 M solution of LRB sulfonyl chloride (90 mg, 150 μmol) in 10% (vol/vol) DIPEA in DMF for 1 h. After extensively washing the resin with DMF, CH_2Cl_2, and 10% DIPEA in DMF, the resin was exchanged into CH_2Cl_2. The 4-methyltrityl group on the side chain on the C-terminal lysine was removed with a solution of 3% TFA in CH_2Cl_2 according to the manufacturer's specifications. 6-CO_2H ZP1 was coupled to the lysine side chain as previously reported (12). Subsequently, the resin was extensively washed with DMF, CH_2Cl_2, and 10% DIPEA in DMF, exchanged into CH_2Cl_2, and then air-dried. The dried resin was cleaved by treatment with a TFA mixture (1.5 mL) consisting of TFA, triisopropylsilane, and water [38:1:1 (vol/vol)] for 2 h. All peptides were purified by HPLC using a Zorbax C18 semipreparative column (9.5 × 250 mm) at a flow rate of 3 mL·min^{-1}. LZ9 required two rounds of HPLC purification in order to obtain an analytically pure sample. In the first round, reverse-phase chromatography was performed with a two-buffer solvent system: A consisted of 0.1% (vol/vol) TFA in water; B consisted of 0.1% (vol/vol) TFA in acetonitrile. The product peak, however, also contained an impurity, the mass of which corresponded to LRB-P_9KE. To remove this impurity, the HPLC solvent system was changed to buffer A consisting of 0.1% (vol/vol) acetic acid in water and B consisting of 0.1% (vol/vol) acetic acid in acetonitrile. The peptide mixture was then purified according to the following protocol: isocratic flow, 0–2.5 min, 10% B; linear gradient 1, 2.5–5 min, 10–25% B; linear gradient 2, 5–20 min, 25–50% B. Like fractions from successive runs were pooled, frozen, and lyophilized. The purity of LZ9 was assessed using a Zorbax C18 analytical column (4.6 mm × 250 mm) at a flow rate of 1 mL·min^{-1}, with the same water/acetonitrile/acetic acid solvent system. The identity of LZ9 was confirmed by ESI-MS (positive mode), chemical formula $C_{130}H_{146}Cl_2N_{20}O_{26}S_2$; *m/z* (amu) calcd for $[M+2H]^{2+}$ = 1,269.5, found = 1,269.7; $[M+3H]^{3+}$ = 846.7, found = 847.4; $[M+4H]^{4+}$ = 635.3, found = 635.7. Five millimolar stocks of LZ9 were prepared in anhydrous DMSO and stored in the dark at −20 °C.

Synthesis of 3-CO_2H CM2. 3-CO_2H CM2 was synthesized by a modified literature procedure (13). Briefly, a suspension of 2,4-DPA (132 mg, 0.66 mmol) and paraformaldehyde (18 mg, 0.6 mmol) in 5 mL of CH_3CN was heated to reflux until the solution clarified (~10 min). The temperature of the oil bath was reduced to 60 °C and a suspension of 7-hydroxycoumarin-3-carboxylic acid (100 mg, 0.485 mmol) in 5 mL CH_3CN was added to the solution. The resulting mixture was heated at 60 °C for 2 h and the crude reaction mixture was cooled to room temperature. A brown solid, the mass (by ESI-MS) of which corresponded to unreacted 7-hydroxycoumarin-3-carboxylic acid, was filtered off. The filtrate was diluted with 20 mL of water, frozen, and lyophilized. The resulting crude solid was purified by reverse-phase HPLC, using the following two-solvent system: Solvent A consisted of 0.1% (vol/vol) TFA in water and B consisted of 0.1% TFA in CH_3CN. The 3-CO_2H CM2 was purified according to the following protocol: isocratic flow, 10% B, 0–5 min, linear gradient, 10–25% B, 5–15 min. Like fractions from successive runs were pooled, frozen, and lyophilized. The retention time was 16 min. The purity of 3-CO_2H CM2 was assessed by analytical HPLC. Yield: 10 mg (4.9%). ^{1}H NMR (500 MHz, DMSO-d_6) δ: 8.74 (d, 2H, J = 6.55), 8.65 (d, 1H, J = 5.66), 8.63 (s, 1H), 8.13 (dt, 1H, J = 7.85, 1.43), 8.00 (d, 2H, J = 6.77), 7.84 (d, 1H, J = 7.9), 7.61 (m, 2H), 4.07 (s, 2H), 4.05 (s, 2H) 3.89 (s, 2H). HRMS (ESI; positive mode), chemical formula: $C_{23}H_{19}N_3O_5$; *m/z* (amu) calcd for $[M+H]^+$ = 418.1397, found = 418.1398. Stock solutions of 3-CO_2H CM2 in DMSO were prepared in the 1.0–10.0 mM range, stored at −20 °C in 50- to 100-μL aliquots, and thawed immediately before each experiment.

Photophysical and Zinc-Binding Properties of LZ9. Spectroscopic measurements were carried out in aqueous buffer (50 mM PIPES 100 mM KCl; pH 7). All buffers were treated with Chelex 100 resin. Emission spectra represent the average of three scans. The $K_{d\text{-}Zn}$ was calculated by fitting the resulting binding isotherm to a single-site model using DynaFit. The metal ion selectivity of LZ9 was assessed using a modified literature procedure (11). The fluorescence spectrum of a 1 μM solution of LZ9 in buffer was acquired before and after addition of a given metal salt stock solution (800 μM $CaCl_2$ or $MgCl_2$; 20 μM $MnSO_4$, $CoCl_2$, $NiCl_2$, $CuCl_2$, or $CdCl_2$). Next, 10 μM $ZnSO_4$ was added and the fluorescence spectrum was measured. Fluorescence signals were integrated and normalized to the integrated signal the metal-free peptide construct (11).

Photophysical and Zinc-Binding Properties of 3-CO_2H CM2. Spectroscopic measurements were carried out in aqueous buffer (50 mM PIPES, 100 mM KCl, pH 7, unless otherwise indicated). Fluorescence data were obtained by exciting at 355 nm and acquiring from 400 to 550 nm. A 0.1-s integration time was used for all fluorescence data and emission spectra represent the average of three scans. To assess the fluorescence response of 3-CO_2H CM2 to added zinc, a 2-mL solution of 10 μM sensor in PIPES buffer at 25 °C was prepared and the fluorescence emission measured. A 2-μL aliquot of 100 mM $ZnSO_4$ (10 equivalents) was added and the fluorescence spectrum acquired, ensuring that the maximum fluorescence intensity had been reached. The quantum yield was determined by referencing sensor solutions to quinine sulfate [λ_{ex} = 360 nm; Φ = 0.577; 0.1 M $H_2SO_{4(aq)}$] (14). The apparent zinc-binding affinity ($K_{d\text{-}Zn}$) of 3-CO_2H CM2 was determined by using a buffer (50 mM Pipes, 100 mM KCl, pH 7). Aliquots of $ZnSO_4$ were successively added to a 10 μM solution of 3-CO_2H CM2. After addition of each aliquot, the solution was allowed to reach equilibrium (*ca*. 3 min). The emission spectrum was then recorded (λ_{ex} = 360 nm; λ_{em} = 400–600 nm). The zinc-binding isotherm was generated by plotting the change in integrated emission intensity (ΔF) as a function of total $ZnSO_4$ concentration. The $K_{d\text{-}Zn}$ was calculated by fitting the resulting binding isotherm to a single-site model using DynaFit.

Mammalian Cell Culture, Labeling, and Imaging Procedures. HeLa cells were cultured at 37 °C under a humidified atmosphere of 5% CO_2 in high-glucose DMEM (Life Technologies) supplemented with 10% (vol/vol) FBS (HyClone), penicillin (100 μg·mL^{-1}), and streptomycin (100 μg·mL^{-1}). For live cell imaging, cells were seeded in 35-mm poly-D-Lys coated glass-bottom culture dishes (MatTek Corporation) 48 h before imaging. Imaging experiments were performed using a Zeiss Axiovert 200M inverted epifluorescence microscope equipped with an EM-CCD digital camera (Hamamatsu) and a MS200 XY Piezo Z stage (Applied Scientific Instruments). The light source was an X-Cite 120 metal-halide lamp (EXFO). Fluorescence images were obtained using an oil-immersion objective at 63× magnification. The microscope was operated using Volocity software (Perkin-Elmer). To measure the cell impermeance of LZ9, HeLa cells were pretreated with

dye- and serum-free medium supplemented with LZ9 (2 μM) and Hoechst 33258 (20 μM) for 30 min (5% CO_2, 37 °C). The plates were then washed with 2 × 1 mL dye- and serum-free DMEM and imaged by multichannel fluorescence microscopy. After initial images were acquired, the medium was replaced on the microscope stage with medium containing zinc pyrithione (25 μM) and the image acquisition process was repeated.

Tricine Potentiometric Titrations. Potentiometric titrations were performed with a Mettler Toledo T70 automated titrator equipped with a DG-111-SG glass electrode calibrated against standard buffers and operated by the LabX-light software. The water-jacketed titration vessel was maintained at 25.0 ± 0.5 °C by a regulated circulating water bath. For each titration, a sample of tricine was predissolved in a known excess of HCl and diluted with Milli-Q water in the titration vessel (30 mL). The final concentration of tricine was 1 mM. All measurements were conducted in the presence of 100 mM KCl to maintain constant ionic strength. Solutions were titrated with 0.1 M NaOH, which was prepared with degassed Milli-Q water and standardized with potassium hydrogen phthalate before each series of titrations. Data analysis was performed with HYPERQUAD2008, using a log K_W value of 13.77. Zinc binding constants were determined from titrations performed in the presence of 0.5 or 1 equivalents of $ZnCl_2$, using the measured pK_a value of tricine (8.06). All reported constants represent averages of the results obtained from a minimum of three independent runs. Speciation plots and titration simulations were built with HySS2009. Beta values were determined by the following equation:

$$\beta_{pqr} = \frac{[M_p L_q H_r]}{[M]^p [L]^q [H]^r},$$

where M = Zn, L = tricine, and H = protons. Log β values are converted to log K values for the formation of each species according to the following expressions:

$$\log\left(K_{Zn}^{ZnLH_{-1}}\right) = \log(\beta_{11-1}); \log\left(K_{ZnLH_{-1}}^{ZnLH_{-2}}\right) = \log\left(K_{Zn}^{ZnLH_{-1}}\right) - \log(\beta_{11-2});$$
$$\log\left(K_{ZnL_2}^{ZnL_2H_{-1}}\right) = \log(\beta_{120}) - \log(\beta_{12-1}); \log\left(K_{ZnLH_{-1}}^{ZnL_2H_{-2}}\right) = \log(\beta_{12-2}) - \log\left(K_{Zn}^{ZnLH_{-1}}\right);$$
$$\log\left(K_{ZnL_2H_{-2}}^{ZnL_2H_{-3}}\right) = \log(\beta_{12-2}) - \log(\beta_{12-3}); \log\left(K_{ZnL_2H_{-3}}^{ZnL_2H_{-4}}\right) = \log(\beta_{12-3}) - \log(\beta_{12-4}).$$

A conditional $K_{d,app}$ value for zinc binding to tricine at pH 7.4 was calculated using HySS2009 according to the following equation:

Let $ZnLH_{-1}$, ZnL_2, *or* $ZnL_2H_{-2} = ZnL$

$$K'_{ZnL} = \frac{[ZnLH_{-1}][ZnL_2H_{-1}][ZnL_2H_{-2}]}{[Zn][L]},$$

where [Zn] = total zinc not bound to L, [L] = total L not bound to zinc, and $K_{d,app} = 1/K'_{ZnL}$. The zinc–tricine complexes $ZnLH_{-1}$, ZnL_2H_{-1}, and ZnL_2H_{-2} were chosen because, based on the speciation plots shown in Fig. S2 *C* and *D*, these are the only forms present at pH 7.4. The $K_{d,app}$ was calculated using experimental data for 1:1 zinc:tricine (1 mM zinc, 1 mM tricine).

Fluorescence Analysis of Competitive Zinc Binding Between Fluorescent Sensors and Zinc Chelators. To assess the ability of each chelator to compete with selected fluorescent zinc sensors, fluorescence spectroscopy was used. For ZPP1 [available from previous studies (15, 16)] fluorescence data were obtained by exciting at 495 nm and acquiring from 500 to 650 nm. For each chelator, a 2-mL solution of 1 μM ZPP1 in PIPES buffer at pH 7.4 was prepared and the initial fluorescence recorded; 2 μM $ZnSO_4$ was added to this solution and the fluorescence intensity measured. To one of these solutions, 10 mM tricine, 50 mM tricine, and 100 mM tricine were successively added and the fluorescence intensity measured. To two other identical solutions, 100 μM CaEDTA and 100 μM ZX1, were added and the final fluorescence intensity was measured for up to 100 s. For 3-CO_2H CM2, a 2-mL solution of 10 μM 3-CO_2H CM2 in Pipes buffer at pH 7.4 was prepared and the initial fluorescence recorded; 4 μM $ZnSO_4$ was added to this solution and the fluorescence intensity measured. To one of these solutions, 100 μM and 10 mM tricine were successively added and the final fluorescence spectrum measured. To two other separate solutions, 100 μM CaEDTA and 100 μM ZX1, were added and the final fluorescence intensity was measured after assuring that a minimum signal was attained. Fluorescence data were integrated and normalized relative to the initial intensity. For both sensors, these experiments were reproduced in Pipes buffer at pH 7.0, and nearly identical results were obtained.

Stopped Flow Fluorescence Studies. Single-mixing stopped flow kinetics studies were performed with a Hi-Tech SF-61 DX2 double-mixing stopped flow apparatus equipped with a fluorescence detector. For experiments with 3-CO_2H CM2, the excitation wavelength was 355 nm. A WG360 glass cutoff filter was placed over the exit to the photomultiplier tube, and emission was monitored from 380 to 700 nm. For experiments with ZPP1, the excitation wavelength was 495 nm and a GG495 glass cutoff filter was used. Emission was monitored from 500 to 700 nm. All solutions were prepared in 50 mM Pipes and 100 mM KCl, pH 7.0, buffer. All measurements were conducted at 25.0 ± 0.1 °C, regulated by a circulating water bath. The temperature inside the sample chamber was monitored with an internal thermocouple.

Determination of Rate Constants for Zinc Binding to 3-CO_2H CM2. To determine the rate of zinc binding to 3-CO_2H CM2, the concentration of zinc was varied and multiple measurements were taken at each concentration using single-mixing stopped flow. A solution of 2 μM 3-CO_2H CM2 was prepared in PIPES buffer at pH 7.0 and solutions of $ZnSO_4$ with concentrations of 200 μM to 1,200 μM were prepared in the same buffer. Measurements were taken at 25 °C. The concentrations after mixing were 1 μM 3-CO_2H CM2 and 100 μM to 600 μM zinc. Using excess zinc in all experiments maintained conditions for pseudo-first-order kinetics. Data were fitted in Prism5 (GraphPad) using the built-in one-phase association equation.

Kinetics of Zinc Binding to Chelators by Competition with 3-CO_2H CM2. To determine the rate at which each chelator removes zinc from a solution of Zn(3-CO_2H CM2), the concentration of chelator was varied and multiple measurements were taken at each concentration. For all chelators, a solution of 20 μM 3-CO_2H CM2 and either 2 or 4 μM $ZnSO_4$ was prepared in PIPES buffer at pH 7.0. Conditions for pseudo-first-order kinetics were maintained by using excess chelator in all experiments. For ZX1 measurements, solutions of ZX1 with concentrations of 20 μM to 240 μM were prepared in the same buffer. Tricine solutions were prepared with concentrations of 8 mM to 32 mM in PIPES. EDTA solutions of 0.48 mM to 4.0 mM were also prepared in PIPES buffer. For all solutions, the after-mixing concentrations were half of the amounts listed above. Data were fitted in Prism5 (GraphPad) using the built-in one-phase decay equation.

Determination of Rate Constants for Zinc Binding to ZPP1. To determine the rate of zinc binding to ZPP1, the concentration of zinc was varied and multiple measurements were taken at each concentration using single-mixing stopped flow. A solution of 2 μM

ZPP1 was prepared in PIPES buffer at pH 7.0 and solutions of $ZnSO_4$ with concentrations of 20 μM to 600 μM were prepared in the same buffer. Measurements were taken at 25 °C. The concentrations after mixing were 1 μM ZPP1 and 10 μM to 300 μM zinc. Using at least a 10-fold excess of zinc in all experiments maintained conditions for pseudo-first-order kinetics. Data were fitted in Prism5 (GraphPad) using the built-in one-phase association equation.

Kinetics of Zinc Binding to ZPP1 in the Presence of Excess Chelators. To determine the effect of excess chelator on the rate and extent of zinc binding to ZPP1, solutions of 50 μM $ZnSO_4$ alone (concentration after mixing) or in the presence of chelator were added to a solution of ZPP1 (1 μM after mixing) and the fluorescence turn-on measured by stopped flow spectroscopy. The tricine concentration (after mixing) was varied from 2 to 16 mM, while holding the concentration of zinc and ZPP1 constant. The amount of tricine in solution was always in excess of zinc. The concentration of ZX1 was varied from 25 μM to 150 μM. The concentration of CaEDTA was varied from 20 to 125 μM.

Values for Main Figures. Fig. 1*F*: Baseline (pC) vs. TBOA (pC): 0.2 Hz: 33.4 ± 19.4 vs. 40.1 ± 10.2 pC, $P = 0.036$; 1 Hz: 39.0 ± 16.5 vs. 56.1 ± 17.8 pC, $P = 0.046$; 5 Hz: 70.9 ± 16.7 vs. 159.3 ± 32.0, $P = 0.004$; 20 Hz: 89.6 ± 18.8 vs. 276.1 ± 47.9 pC, $P = 0.002$; 50 Hz: 105.35 ± 16.8 vs. 343.4 ± 61.5 pC, $P = 0.002$; 100 Hz: 110.77 ± 10.6 vs. 372.5 ± 64.4 pC, $P = 0.003$; 150 Hz: 148.66 ± 35.8 vs. 366.8 ± 59.4 pC, $P = 0.002$; paired *t* tests, $n = 7$.

Fig. 1*H*: (*Right*) Baseline tau = 0.34 ± 0.01 s, D-AA tau = 0.26 ± 0.01 s, $P = 0.01$, paired *t* test, $n = 4$.

Fig. 1*I*: (*Right*) Baseline tau = 0.33 ± 0.02 s, CPP tau = 0.32 ± 0.02 s, $P = 0.17$, paired *t* test, $n = 4$.

Fig. 2*B*: one micromolar ZPP1 with 2 μM zinc: 4.37 ± 0.08. Plus: 10 mM tricine: 2.92; 50 mM tricine: 1.72; 100 mM tricine: 1.38; 100 μM CaEDTA: 0.971; 100 μM ZX1: 0.983.

Fig. 2*C*: ten micromolar 3-CO_2H CM2 with 4 μM zinc: 1.19 ± 0.02. Plus: 100 μM tricine: 1.16; 10 mM tricine: 0.998; 100 μM CaEDTA: 0.997; 100 μM ZX1: 0.976.

Fig. 2*D*: k_{obs} values (s^{-1}). ZX1: 10 μM = 10.7 ± 0.2, 25 μM = 17.9 ± 0.3, 40 μM = 28.4 ± 0.7, 80 μM = 42 ± 1, 100 μM = 48 ± 5, 120 μM = 57 ± 1. Tricine: 4 mM = 22.8 ± 0.7, 6 mM = 27.6 ± 0.6, 8 mM = 33.4 ± 0.9, 10 mM = 41 ± 7, 12 mM = 40 ± 1, 16 mM = 47 ± 1. CaEDTA: 240 μM = 7.4 ± 0.2, 480 μM = 8.0 ± 0.2, 720 μM = 8.5 ± 0.2, 960 μM = 8.9 ± 0.2, 2,000 μM = 11.3 ± 0.6.

Fig. 3*C*: WT, $n = 8$, compared with ZnT3 KO, $n = 6$: 5 Hz: 40.2 ± 7.1% vs. 5.8 ± 8.4%, $P = 0.008$; 20 Hz: 34 ± 5.4% vs. 5.4 ± 3.7%, $P = 0.01$, *t* tests.

Fig. 3*D*: $n = 5$ for both; 5 Hz: 0.79 ± 0.18 vs. 0.81 ± 0.20 μM, $P = 0.93$; 20 Hz: 0.64 ± 0.12 vs. 0.64 ± 0.09 μM, $P = 0.99$, *t* tests.

Fig. 3*F*: $\tau_{D\text{-}AA}/\tau_{baseline}$, 5 Hz: WT = 100.7 ± 0.6%, $n = 4$ vs. KO = 97.2 ± 4.9%, $n = 4$, $P = 0.86$, rank sum test; 20 Hz: WT = 79.7 ± 1.6% vs. KO = 76.6 ± 4.1%, $P = 0.81$, *t* test.

Fig. 4*F*: WT = 0.59 ± 0.06%, $n = 11$, ZnT3 KO = -0.01 ± 0.01%, $n = 5$, rank sum test, $P = 0.0002$.

Fig. 4*H*: WT = 0.8 ± 0.3 nM, $n = 5$, ZnT3 KO = 1.0 ± 0.2 nM, $n = 6$, *t* test, $P = 0.6$.

Fig. 4*I*: LZ9 = 43.2 ± 3.6% n = 11, NG = 0.1 ± 1.8% n = 4, *t* test, $P = 0.001$.

Fig. 5*B*: n = 8, 5 Hz: 40.2 ± 7.1% $P = 0.0008$; 20 Hz: 34.3 ± 5.4%, $P = 0.0004$; 100 Hz: 21.7 ± 4.5%, $P = 0.002$; 150 Hz: 14.8 ± 3.8%, $P = 0.006$, paired *t* tests vs. control (no ZX1).

Fig. 5*C*: low vs. high 37.3 ± 4.3% vs. 18.3 ± 3.0%, $P = 0.0001$, paired *t* test.

Fig. 5*E*: $n = 6$, 5 Hz: 5.8 ± 8.4%, $P = 0.522$; 20 Hz: 5.4 ± 3.7%, $P = 0.20$; 100 Hz: 16.7 ± 2.5%, $P = 0.001$; 150 Hz: 13.2 ± 2.5%, $P = 0.003$, paired *t* tests.

WT ($n = 8$) vs. KO ($n = 6$): 5 Hz: 40.2 ± 7.1% vs. 5.8 ± 8.4%, $P = 0.008$; 20 Hz: 34 ± 5.4% vs. 5.4 ± 3.7%, $P = 0.01$; 100 Hz: 21.7 ± 4.5% vs. 16.7 ± 2.5%, $P = p = 0.394$; 150 Hz: 14.8 ± 3.8% vs. 13.2 ± 2.5%, $P = 0.748$, *t* tests.

Fig. 5*F*: low vs. high 5.6 ± 4.4% vs. 15.0 ± 1.8%, $P = 0.034$, paired *t* test.

Fig. 5*I*: KO vs. control ($n = 5$): 28 ± 7.8%, $P = 0.0023$, paired *t* test. WT vs. control ($n = 11$): 16.2 ± 5.9%, $P = 0.007$, paired *t* test. KO vs. WT, $P = 0.21$, rank sum test.

Fig. 6*B*: ZX1 in TBOA ($n = 9$) vs. ZX1 alone ($n = 6$); 5 Hz: 33.4 ± 10.9% vs. 5.8 ± 8.4%, $P = 0.033$; 20 Hz: 31.8 ± 7.6% vs. 5.4 ± 3.7%, $P = 0.005$; 100 Hz: 18.3 ± 5.4% vs. 16.7 ± 2.5%, $P = 0.399$; 150 Hz: 18.7 ± 6.2 vs. 13.2 ± 2.5%, $P = 0.214$, *t* tests.

Fig. 6*C*: compared with ZnT3 KO: WT ($n = 7$), 5 Hz: 45.1 ± 14.8%, $P = 0.943$; 20 Hz: 27.3 ± 8.8%, $P = 0.811$; 100 Hz: 21.7 ± 7.3%, $P = 0.881$; 150 Hz: 20.9 ± 7.0%, $P = 0.935$, *t* tests.

1. Suter BA, et al. (2010) Ephus: Multipurpose data acquisition software for neuroscience experiments. *Front Neural Circuits* 4:100.
2. Tovar KR, Westbrook GL (2012) Amino-terminal ligands prolong NMDA receptor-mediated EPSCs. *J Neurosci* 32(23):8065–8073.
3. Hansen KB, Ogden KK, Yuan H, Traynelis SF (2014) Distinct functional and pharmacological properties of Triheteromeric GluN1/GluN2A/GluN2B NMDA receptors. *Neuron* 81(5):1084–1096.
4. Pan E, et al. (2011) Vesicular zinc promotes presynaptic and inhibits postsynaptic long-term potentiation of mossy fiber-CA3 synapse. *Neuron* 71(6):1116–1126.
5. Woodroofe CC, Masalha R, Barnes KR, Frederickson CJ, Lippard SJ (2004) Membrane-permeable and -impermeable sensors of the Zinpyr family and their application to imaging of hippocampal zinc in vivo. *Chem Biol* 11(12):1659–1666.
6. Middleton JW, et al. (2011) Mice with behavioral evidence of tinnitus exhibit dorsal cochlear nucleus hyperactivity because of decreased GABAergic inhibition. *Proc Natl Acad Sci USA* 108(18):7601–7606.
7. Grynkiewicz G, Poenie M, Tsien RY (1985) A new generation of Ca2+ indicators with greatly improved fluorescence properties. *J Biol Chem* 260(6):3440–3450.
8. Park JG, Palmer AE (2014) Quantitative measurement of Ca2+ and Zn2+ in mammalian cells using genetically encoded fluorescent biosensors. *Methods Mol Biol* 1071: 29–47.
9. Yang H, Vasudevan S, Oriakhi C, Shields J, Carger R (2008) Scalable synthesis of lissamine rhodamine B sulfonyl chloride and incorporation of xanthene derivatives onto polymer supports. *Synthesis* 2008(6):957–961.
10. Wong BA, Friedle S, Lippard SJ (2009) Solution and fluorescence properties of symmetric dipicolylamine-containing dichlorofluorescein-based Zn2+ sensors. *J Am Chem Soc* 131(20):7142–7152.
11. Chyan W, Zhang DY, Lippard SJ, Radford RJ (2014) Reaction-based fluorescent sensor for investigating mobile Zn2+ in mitochondria of healthy versus cancerous prostate cells. *Proc Natl Acad Sci USA* 111(1):143–148.
12. Radford RJ, Lippard SJ (2013) Chelators for investigating zinc metalloneurochemistry. *Curr Opin Chem Biol* 17(2):129–136.
13. Mizukami S, Okada S, Kimura S, Kikuchi K (2009) Design and synthesis of coumarin-based Zn(2+) probes for ratiometric fluorescence imaging. *Inorg Chem* 48(16):7630–7638.
14. Lakowicz J (2006) *Principles of Fluorescence Spectroscopy* (Springer, New York), p 3.
15. Buccella D, Horowitz JA, Lippard SJ (2011) Understanding zinc quantification with existing and advanced ditopic fluorescent Zinpyr sensors. *J Am Chem Soc* 133(11): 4101–4114.
16. Zhang XA, Hayes D, Smith SJ, Friedle S, Lippard SJ (2008) New strategy for quantifying biological zinc by a modified zinpyr fluorescence sensor. *J Am Chem Soc* 130(47): 15788–15789.

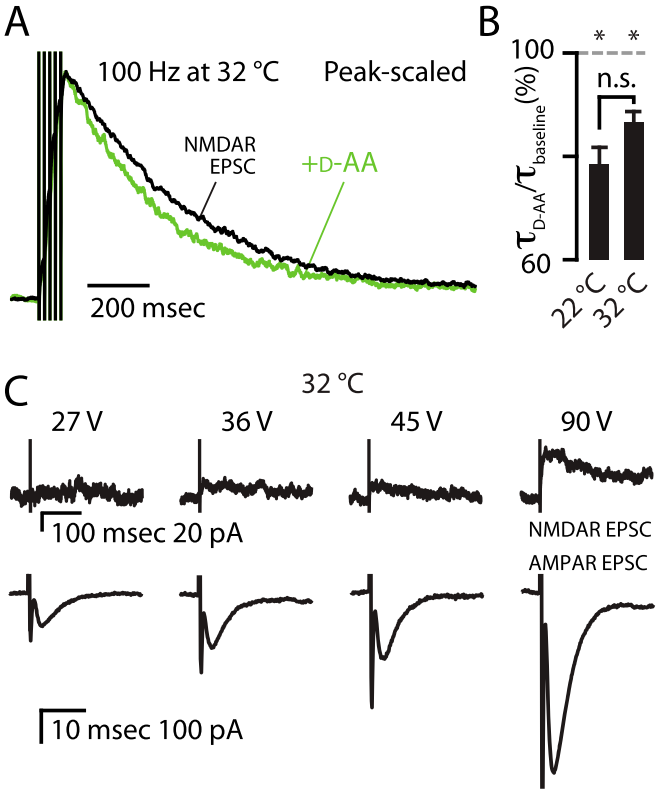

Fig. S1. Glutamate spillover and pooling occur at 32 °C. (*A*) At 32 °C, peak-scaled NMDAR EPSCs following a five-pulse, 100-Hz train stimulus showed that D-AA (70 μM) sped the decay tau. (*B*) Group data showed that the effect of D-AA on the decay kinetics of NMDAR EPSCs were not different between 32 °C and 22 °C ($\tau_{D\text{-}AA}/\tau_{baseline}$): 22 °C: 78.5 ± 3.3% $P = 0.007$, $n = 4$; 32 °C: 86.3 ± 2.4%, $P = 0.002$ paired *t* tests, $n = 5$; 22 °C vs. 32 °C, $P = 0.09$, *t* test. (*C*) At 32 °C, single electrical pulses elicited an AMPAR EPSC at lower stimulus intensity compared with the stimulus intensity required for eliciting an NMDAR EPSC. Error bars represent SEM.

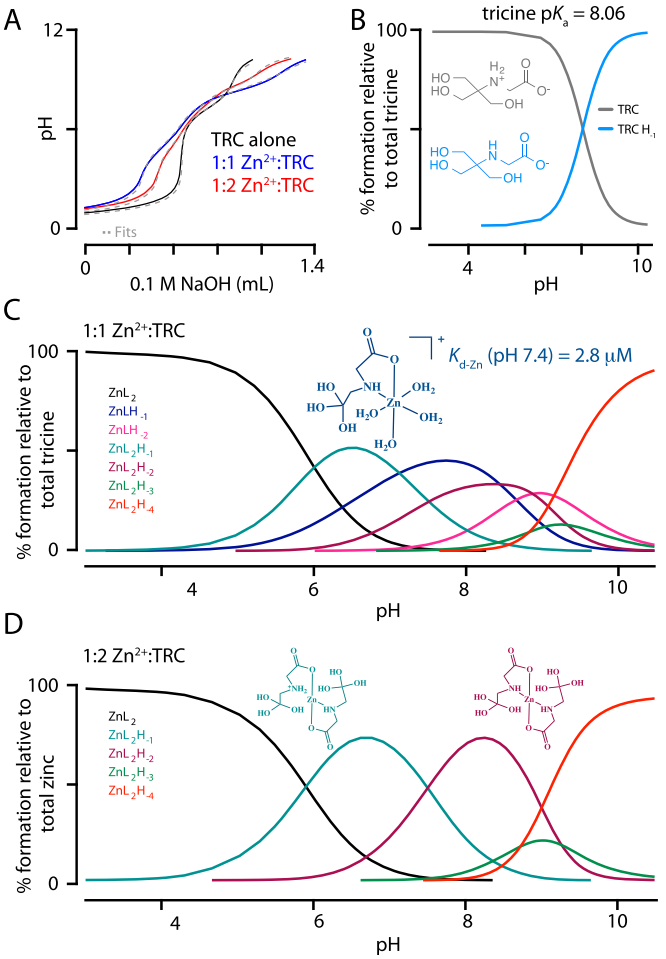

E

Zn^{2+}-tricine species (p, q, r)	log β (M^{-1})	log K (M^{-1})
LH_{-1} (0, 1, -1)	-8.06 ± 0.07	8.06
$ZnLH_{-1}$ (1, 1, -1)	6.66 ± 0.03	6.66
$ZnLH_{-2}$ (1, 1, -2)	-1.96 ± 0.01	8.62
ZnL_2 (1, 2, 0)	26.1 ± 0.1	N.A.
ZnL_2H_{-1} (1, 2, -1)	20.1 ± 0.1	6.00
ZnL_2H_{-2} (1, 2, -2)	12.51 ± 0.01	5.85
ZnL_2H_{-3} (1, 2, -3)	3.2 ± 0.1	9.31
ZnL_2H_{-4} (1, 2, -4)	-5.60 ± 0.01	8.80

Fig. S2. Zinc-binding properties of tricine. (*A*) Potentiometric titration curves for tricine (TRC) alone (black), tricine with 1/2 equivalent zinc (red), and with 1 equivalent zinc (blue) from average estimated pK_a values. Calculated curves are shown overlaid (gray lines). The log β value determined from fitting tricine alone was used as a constant for fitting data in the presence of zinc. The stability constants derived from fitting data for tricine with 1/2 equivalent of zinc were used as constants for fitting data for tricine with 1 equivalent of zinc. (*B*) Calculated speciation diagram for the tricine alone titration shown in *A*. Conditions: 1.0 mM tricine in 100 mM KCl at 25 °C, treated with a known excess of HCl and titrated with 0.1 M NaOH. (*C*) Relative species formation for tricine + 1 equivalent zinc. Conditions: 1.0 mM tricine and 1.0 mM $ZnCl_2$ in 100 mM KCl at 25 °C, treated with a known excess of HCl and titrated with 0.1 M NaOH. (*D*) Relative species formation for tricine + 1/2 equivalent zinc. The $K_{d\text{-}Zn}$ (apparent at pH 7.4) is shown in the inset and represents all relevant zinc–tricine complexes at pH 7.4 (1:1 and 1:2 zinc:tricine complexes are present). Conditions: 1.0 mM tricine and 0.5 mM $ZnCl_2$ in 100 mM KCl at 25 °C, treated with a known excess of HCl and titrated with 0.1 M NaOH. (*E*) pH-independent overall (β) and stepwise (K) stability constants for tricine and various zinc–tricine complexes as determined by fitting potentiometric titration data at 25 °C.

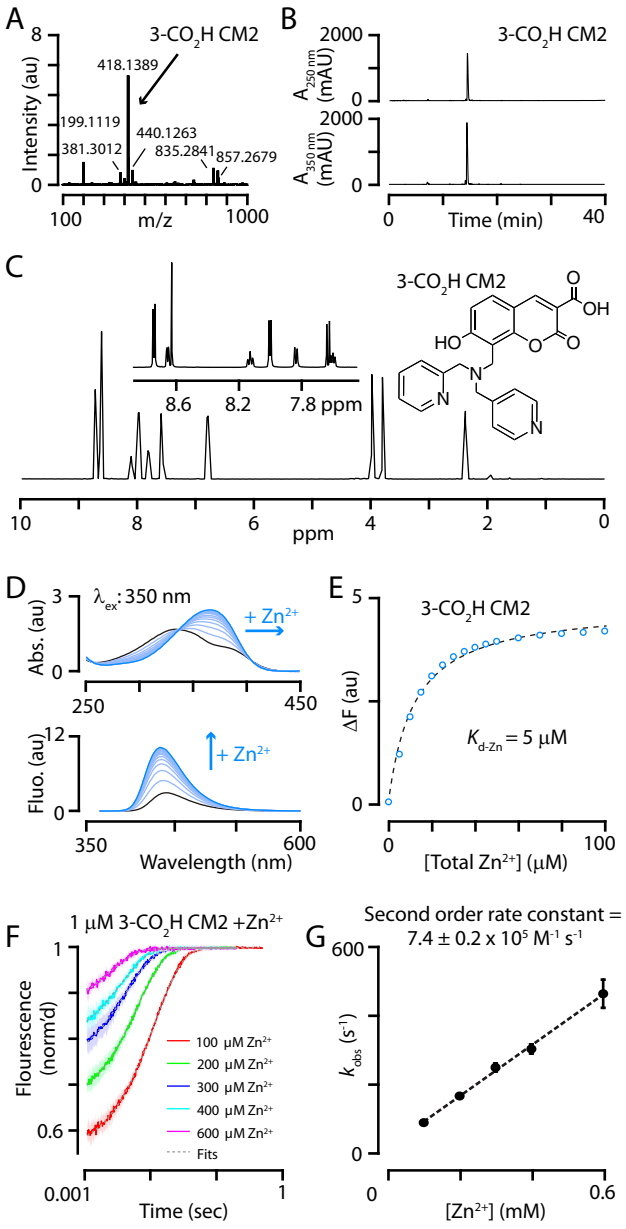

Fig. S3. Synthesis and characterization of 3-CO_2H CM2. (*A*) HR-ESI-MS of 3-CO_2H CM2. (*B*) Analytical HPLC chromatograms of 3-CO_2H CM2. (*C*) The ^{1}H NMR (500 MHz, DMSO-d_6) spectrum of 3-CO_2H CM2. (*D*) Changes in the absorbance (*Top*) and emission (*Bottom*) spectra of a 19 μM solution of 3-CO_2H CM2 in buffer upon addition of successive aliquots of $ZnSO_4$. (*E*) A representative binding isotherm and fit for titration of $ZnSO_4$ into a solution of 3-CO_2H CM2. λ_{ex} = 360 nm. (*F*) Determination of rate constants for zinc binding to 3-CO_2H CM2. Stopped flow fluorescence kinetic traces and monoexponential fits for zinc binding to 1 μM 3-CO_2H CM2. Fluorescence data are normalized to the maximum fluorescence of Zn(3-CO_2H CM2). (*G*) Plot of observed pseudo-first-order rate constants vs. [zinc] from *F*. The slope of the linear fit is taken as the second-order rate constant, k_2 = 7.4 (± 0.2) × 10^5 $M^{-1}{\cdot}s^{-1}$. Data were collected in aqueous buffer (50 mM PIPES and 100 mM KCl, pH 7.0) at 25 °C. Error bars represent SD.

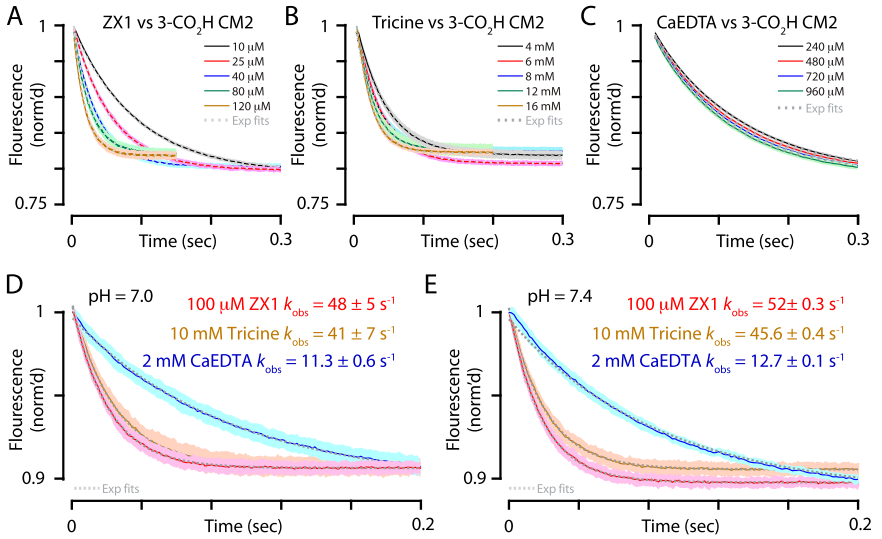

Fig. S4. Detailed kinetic analysis for zinc binding to ZX1, tricine, and CaEDTA by competition with 3-CO_2H CM2. (*A*) Kinetic traces and rate constant fits of various concentrations of ZX1 competing for zinc from 4 μM Zn(3-CO_2H CM2). (*B*) Kinetic traces and rate constant fits of various concentrations of tricine (TRC) competing for zinc from 4 μM Zn(3-CO_2H CM2). (*C*) Kinetic traces for rate constant fits of various concentrations of CaEDTA competing for zinc from 4 μM Zn(3-CO_2H CM2). (*D*) Overlay of selected kinetic traces as in *A*–*C* fitted with monoexponential functions for competition against 2 μM Zn(3-CO_2H CM2) at pH 7.0. (*E*) Traces as in *D*, but at pH 7.4. All fluorescence data are normalized to the initial fluorescence level of Zn(3-CO_2H CM2). All data were collected in aqueous buffer (50 mM PIPES and 100 mM KCl) at 25 °C.

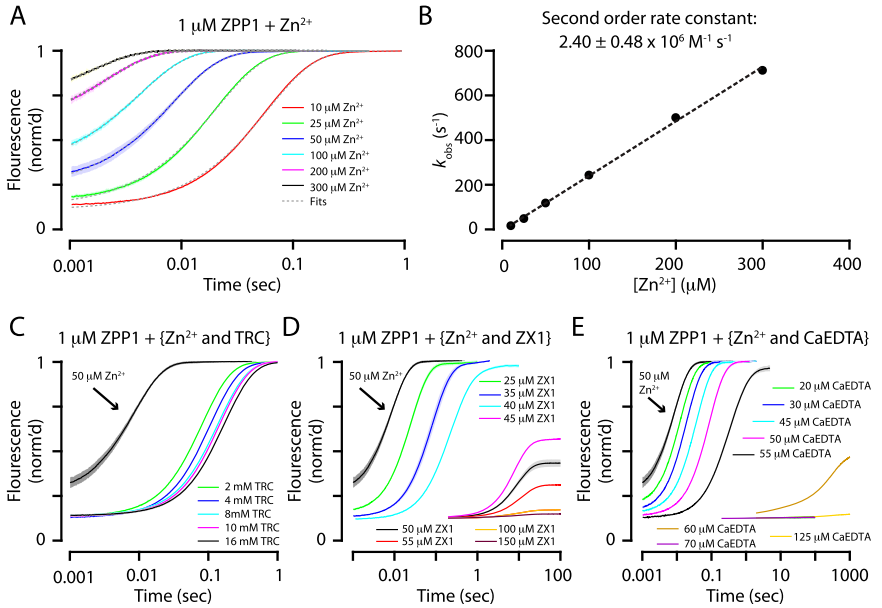

Fig. S5. Detailed analysis of the rate of zinc binding to ZPP1 in the presence of ZX1, tricine, and CaEDTA. (*A*) Determination of rate constants for zinc binding to ZPP1. Stopped flow fluorescence kinetic traces and single exponential fits for zinc binding to 1 μM ZPP1 as a function of zinc concentration. (*B*) Plot of observed pseudo-first-order rate constants from *A* vs. [zinc]. The slope of the linear fit is taken as the second-order rate constant, $k_2 = 2.40\ (\pm\ 0.48) \times 10^6\ M^{-1}{\cdot}s^{-1}$. (*C*) Stopped flow fluorescence kinetic traces showing the change in fluorescence signal from 1 μM ZPP1 with addition of 50 μM zinc and varied concentrations of tricine. Tricine was unable to prevent the turn-on of ZPP1 at all concentrations tested. (*D*) Same experiment as in *C*, but with ZX1. Consistent with the high $K_{d\text{-}Zn}$ (1 nM), turn-on was observed when zinc was in excess of ZX1 in solution, but little to no turn-on was observed with equimolar or excess ZX1. (*E*) Same experiment as in *C*, but with CaEDTA. Variation of [CaEDTA] from 20 to 125 μM yielded results similar to those in *D*. All fluorescence data are normalized to the fluorescence level of Zn_2ZPP1. Data were collected in aqueous buffer (50 mM PIPES and 100 mM KCl, pH 7.0) at 25 °C.

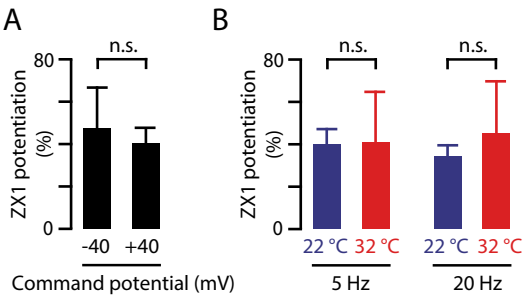

Fig. S6. Synaptic zinc does not modulate the voltage-dependent low-affinity zinc-binding site of NMDARs; zinc chelation with ZX1 modulates extrasynaptic NMDARs at 32 °C. (*A*) Summary graph showing that in response to 5-Hz stimulation and in low extracellular magnesium (200 μM), ZX1 did not have a larger effect on NMDAR EPSCs at −40 mV compared with +40 mV (−40 mV, $n = 6$, ZX1 potentiation = 47.1 ± 20%; +40 mV, replotted from Fig. 3*C*, $n = 8$, ZX1 potentiation = 40.2 ± 7.1%; $P = 0.72$, *t* test). (*B*) Summary graph showing that low frequency trains (5 and 20 Hz) activated NMDAR EPSCs that were equally potentiated by zinc chelation with ZX1 at 22 °C ($n = 8$) and 32 °C ($n = 5$) (5 Hz: 22 °C: 40.2 ± 7.1%, 32 °C: 40.8 ± 24.1%, $P = 0.98$ *t* test; 20 Hz: 22 °C: 34.3 ± 5.4%, 32 °C: 45.6 ± 24.3% $P = 0.58$, *t* test). Error bars represent SEM.

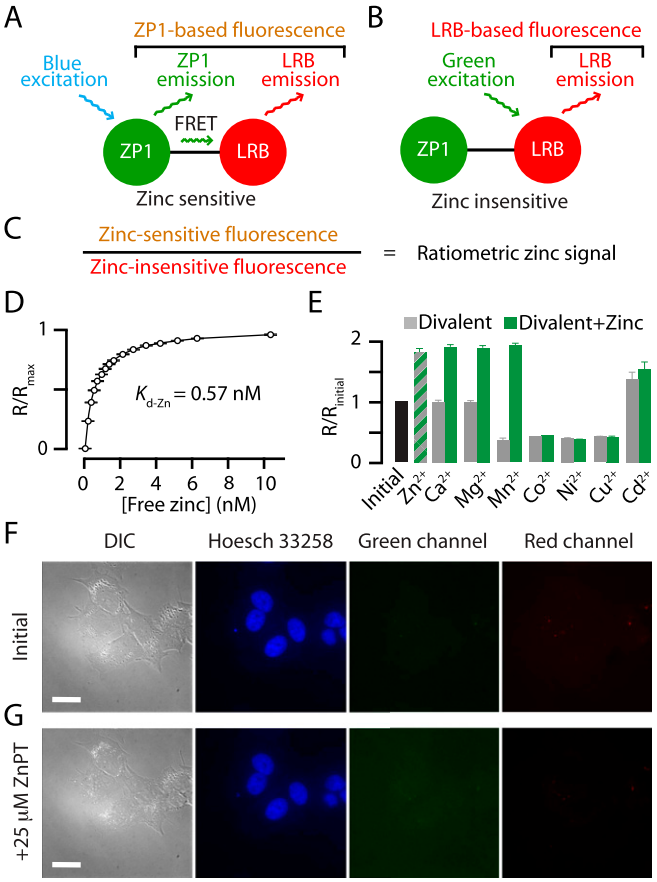

Fig. S7. Chemical properties and characterization of the extracellular ratiometric zinc sensor LZ9. (*A*) Schematic representation of LZ9. Blue excitation activates primarily the zinc-sensitive portion of the molecule (ZP1). This zinc-sensitive fluorescence can be detected as a combination of green emission directly from ZP1 and as red emission from LRB excitation via Förster resonance transfer. Therefore, blue excitation of LZ9 results in zinc-sensitive emission. (*B*) Green illumination of LZ9 primarily activates LRB. Therefore, green excitation of LZ9 results in zinc-insensitive emission. (*C*) The ratio of the zinc-sensitive florescence during blue excitation to zinc-insensitive fluorescence during green excitation is the ratiometric zinc signal. (*D*) Zinc-binding isotherm for the normalized ratiometric response of LZ9. The apparent zinc dissociation constant ($K_{d\text{-}Zn}$) was measured to be 0.57 nM. (*E*) Ratiometric response of LZ9 in response to zinc compared with magnesium, calcium, manganese, cobalt, nickel, copper, and cadmium. Initial fluorescence of the probe (black bar) in pH-buffered medium free from cations. The addition of zinc to the solution increased the ratiometric fluorescence by saturating the probe (gray and green hashed bar). In a separate experiment, $CaCl_2$ was added to the medium and no change in fluorescence from LZ9 occurred (gray bar), but the subsequent addition of zinc increased the fluorescence to the same levels as for zinc alone (green bar), indicating that LZ9 is highly selective for zinc over calcium. The same experimental sequence was performed for $MgCl_2$ with the same result. Magnesium alone caused no change in LZ9 fluorescence (gray bar) and the subsequent addition of zinc saturated the probe and fluorescence increased to the same levels as they had done with zinc alone. We found that, except for cadmium, the ratiometric signal from the probe was selective for zinc over all other divalent metal ions tested. (*F*) To verify that LZ9 remains extracellular, HeLa cells (*Left*) were pretreated with DMEM supplemented with LZ9 (2 μM) and Hoechst 33258 (20 μM, an intracellular fluorescent marker that labels nuclei, *Middle*) for 30 min (5% CO_2, 37 °C). Consistent with LZ9 being cell-impermeable, no intracellular red or green fluorescence was observed under these conditions (*Right*). If LZ9 were cell permeable, we would expect to see fluorescent signals due to intracellular free zinc. (*G*) In case intracellular zinc levels were not detectable by LZ9 under the conditions described in *A*, after initial images were acquired, zinc pyrithione (ZnPT, a zinc ionophore, 25 μM) was added to the medium to increase intracellular zinc levels. No significant fluorescence was observed after addition of ZnPT ($n = 6$), indicating that the lack of fluorescence signal is due to the absence of intracellular LZ9. Error bars represent SD.

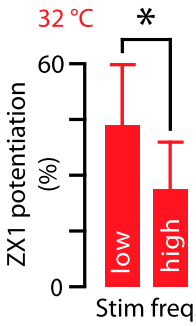

Fig. S8. Zinc chelation with ZX1 is frequency-dependent at 32 °C. Summary graph showing that in WT mice, the difference in zinc chelation between high- (100 Hz and 150 Hz) and low- (5 Hz and 20 Hz) frequency stimulus trains is maintained at 32 °C (low: 42.8 ± 16.9% vs. high 25.9 ± 12.6%, p 0.01, paired *t* test). Error bars represent SEM.

Table S1. D-AA and ifenprodil sensitivity of NMDAR EPSCs in WT and ZnT3 KO mice

	Stimulus frequency, Hz			
NMDAR EPSCs	5	20	100	150
WT				
Ifenprodil IC_{50}, μM, $n = 5$[†]	0.79 ± 0.18	0.64 ± 0.12	0.60 ± 0.13	0.57 ± 0.11
Maximum ifenprodil inhibition, %, $n = 5$	84.1 ± 3.8*	93.7 ± 1.3	95.6 ± 1.2	95.9 ± 1.1
$\tau_{DAA} - \tau_{baseline}$, %, $n = 4$	100.7 ± 4.9*	76.6 ± 4.1	78.5 ± 3.4	78.5 ± 3.1
ZnT3 KO	5	20	100	150
Ifenprodil IC_{50}, μM, $n = 5$[‡]	0.81 ± 0.20 0.94[a]	0.64 ± 0.09 0.99[a]	0.89 ± 0.11 0.12[a]	0.86 ± 0.15 0.16[a]
Maximum ifenprodil inhibition, %, $n = 5$	87.1 ± 2.8 0.54[a]	92.4 ± 1.8 0.56[a]	95.1 ± 1.0 0.97[a]	96.1 ± 1.1 0.89[a]
$\tau_{DAA} - \tau_{baseline}$, %, $n = 4$	97.2 ± 0.6* 0.86[b]	79.7 ± 1.6 0.81[a]	76.5 ± 2.9 0.49[b]	72.0 ± 0.7 0.34[b]

All data were collected in ACSF containing 100 μM ZX1.
[†]$P = 0.76$, one-way ANOVA across stimulus frequencies, within genotype.
[‡]$P = 0.77$, one-way ANOVA across stimulus frequencies, within genotype.
*$P < 0.05$ vs. 20,100, and 150 Hz, paired t tests.
[a]*t* test, *P* value vs. WT.
[b]Rank sum test, *P* value vs. WT.

Table S2. Photophysical and zinc-binding properties of flourescent zinc sensors

	Abs_{max}, nm, ε × 10^4 ($M^{-1}{\cdot}cm^{-1}$)		Em_{max}, nm, Φ		
Sensor	Apo	$+Zn^{2+}$	Apo	$+Zn^{2+}$	$K_{d\text{-}Zn}$, nM
ZPP1[a]	517, 75 ± 5	505, 82 ± 2	532, 0.052	523, 0.70	15.6 ± 4.9
3-CO_2H CM2	348	373	444, 0.33 ± 0.3	437, 0.64 ± 0.9	5,000 ± 1,600
LZ9	520, 11.7 572, 11.4	510, 10.8 570, 11.1	530, 0.080 ± $4e^{-3}$ [b] 590, 0.180 ± $8e^{-3}$ [c]	528, 0.129 ± $7e^{-3}$ 590, 0.250 ± $2e^{-2}$	0.57 ± 0.3[d]
Newport Green[e]	506, 8.2	506, 8.2	535, n.r	535, n.r.	1,000

All measurements were made in buffer (50 mM PIPES and 100 mM KCl, pH 7). Values are presented as mean ± SD. ε, extinction coefficient; Φ, quantum yield; Abs_{max}, peak of absorption spectrum; Apo, metal-free state; Em_{max}, peak of emission spectrum; n.r.: not recorded. See *SI Materials and Methods* for details.
[a]Values taken from ref. 1.
[b]Quantum yields were measured using a solution of fluorescein in 0.1 M $NaOH_{aq}$ (Φ = 0.95) (2) as a standard. Fluorescence spectra were integrated from 500 to 700 nm.
[c]Quantum yields were measured using a solution of rhodamine B in ethanol (Φ = 0.49) (3) as a standard. Fluorescence spectra were integrated from 550 to 700 nm.
[d]Apparent dissociation constant ($K_{d\text{-}Zn}$) was measured in the presence of EGTA as a competing ligand.
[e]Data taken from ref. 4.

1. Buccella D, Horowitz JA, Lippard SJ (2011) Understanding zinc quantification with existing and advanced ditopic fluorescent Zinpyr sensors. *J Am Chem Soc* 133(11):4101–4114.
2. Lakowicz JR (1999) *Principles of Fluorescence Spectroscopy* (Plenum, New York), 2nd Ed.
3. Casey KG, Quitevis EL (1988) Effect of solvent polarity on nonradiative processes in xanthene dyes: Rhodamine B in normal alcohols. *The Journal of Physical Chemistry* 92(23):6590–6594.
4. Haugland RP, Spence MT, Johnson ID (1996) *Handbook of Fluorescent Probes and Research Chemicals* (Molecular Probes, Eugene, OR).